

USGS Award Number GP15AP00006

**Kinematic and Dynamic Models of the Southern California Lithosphere: Applications to Estimating Crustal Stresses and Stressing Rates**

Elizabeth Hearn, Consulting Geophysicist  
21 Valley Oak Street, Portola Valley CA 94028  
Phone: (408) 334-8075  
Fax: 650-329-5163  
Email: [hearn.liz@gmail.com](mailto:hearn.liz@gmail.com)

**Grant Time Period: January 1, 2015 - December 31, 2015**

**Abstract**

I have developed several suites of kinematic models of southern California to reconcile geodetically-inferred fault slip rates with longer-term geologic rates, and to estimate how much “off-fault” deformation is occurring in this region. Model suites were calibrated to either GPS data or to a strain energy minimization constraint, and either incorporated “locked” faults or did not. All of the models suggest slip rates for the San Gorgonio Pass, North and South Mojave segments of the San Andreas Fault that are at the low end of their UCERF3 ranges. Rates inferred for the Ventura-Oak Ridge fault zone in the Transverse Ranges are below estimates based on summed UCERF3 rates for individual faults, but are consistent with recent geologic estimates (Hubbard et al., 2014). Disagreements between inferred geodetic and longer-term slip rates are significant for the south-central San Jacinto Fault, the Imperial Fault and the Coachella section of the San Andreas fault, and can only be partially reconciled by reducing the locking depths of these features. Correcting the SCEC CMM4 GPS velocity field for seismic cycle effects associated with large earthquakes on the 1857 SAF rupture segment increases the inferred slip rate of the Mojave segment of the San Andreas fault by about 4 mm/yr, but does not appear to affect inferred slip rates on other segments. Off-fault deformation appears to account for 23-32% of the total strain energy accumulation in southern California, depending on how it is calculated. This is in agreement with prior estimates (e.g. Field et al., 2013, Johnson, 2013). Development of dynamic models has been held up by problems with stability of stress-driven fault slip computations on crooked or discontinuous faults. I have implemented plasticity and a more stable type of stress-driven fault slip in my finite-element code, and will pursue dynamic modeling as part of a NEHRP-funded project in 2016.

**Kinematic modeling**

For the kinematic modeling, my efforts centered on implementing a Markov Chain Monte Carlo (MCMC) method to supplement the least squares Monte Carlo method I have used in the past for inverting slip rates. I have also adjusted the SCEC CMM4 GPS velocity field to remove a long-wavelength viscoelastic perturbation resulting from large earthquakes on the 1857 rupture seg-

ment of the SAF, and inverted this velocity field for slip, as a first step in assessing the importance of this transient to inferred slip rates. By varying locking depths (based on UCERF3 data) and accounting for viscoelastic seismic cycle effects, I am working to resolve geologic-geodetic slip rate discrepancies in the kinematic model.

#### MCMC inversion

Until this year, my finite-element deformation code GAEA (Saucier and Humphreys, 1993) was set up to sample slip rates randomly from boxcar or normal distributions and to output scores for all cases (either weighted residual sum of squares (WRSS) misfit to GPS velocities, or total strain energy). I could select the set of fault segment slip rates that give the best solution by each metric, but could not report formal uncertainties in these rates. To address this, I implemented two Markov Chain Monte Carlo (MCMC) methods: Independence sampler MCMC and Random Walk Metropolis-Hastings MCMC. The Independence sampler method involves random sampling of slip rates (within a boxcar range or a truncated normal distribution) but after each case is run, the solution is either accepted or rejected based on how well it fits the GPS velocities (or how low the model strain energy is) compared to the previous solution. Models that better fit the constraints (i.e., have a higher likelihood value) are more likely to be accepted than models that perform more poorly. The next sample of slip rates is randomly drawn from the same distribution as before, regardless of whether the model was accepted or not. The random walk Metropolis-Hastings method takes into account previous guesses by sampling parameters from distributions around values from the most recent accepted model, rather than from pre-ordained distributions. In both cases, the solution becomes insensitive to the initial set of assumed slip rates after a burn-in period, and accepted models should define a probability distribution of slip rates for individual fault segments.

Inferred slip rates appear to be independent of the inversion technique I use - that is, MCMC inversions and least-squares Monte Carlo inversions point to the same preferred slip rate ranges. However, neither of the MCMC methods resolves slip rates as well as the least-squares Monte Carlo approach. I show results for both techniques. To estimate errors, I use the approach described by Johnson (2013, Figure 16), though this approach may be overly conservative.

#### Preliminary kinematic model results

I have run several suites of 10,000 kinematic models, with locked (to depths based on UCERF3 values) or unlocked faults, calibrated to either the SCEC CMM4 GPS velocity field or a strain energy minimization constraint (Figure 1). I describe three suites here: Suite 1 comprises locked models calibrated to the SCEC CMM4 velocity field. Suite 2 comprises unlocked models calibrated to a strain energy minimization constraint. An additional suite of locked models (Suite 1a) is calibrated to a version of the GPS velocity field that has been corrected for viscoelastic seismic cycle effects due to large quakes on the 1857 rupture segment (as done by Hearn et al., 2013). In all cases, fault slip rates are sampled from ranges given in the UCERF3 final report (Table B1 of Field et al., 2013). Monte Carlo least squares and two MCMC methods are used to estimate slip rates (e.g., Figure 1). The models yield clear slip rate preferences for some (though not most!)

fault segments. Weighted residual sum of squares (WRSS) misfits to the GPS velocities are large because of the small formal errors in many of the GPS velocities. Like Johnson (2013), I chose to scale up the formal velocity uncertainties to generate a normalized weighted residual quantity with a minimum value of about 1. I had to scale the one-sigma errors (68% confidence intervals) by a factor of five, and to truncate any values below 0.5 mm/yr (after scaling). Typical misfits are of the order of 1-3 mm/yr. Larger misfits are evident in the areas of the Landers, Hector Mine and El Mayor-Cucapah earthquakes (Figure 2).

*Southern San Andreas Fault system.* Within the UCERF3 slip rate ranges, the GPS-constrained Suite 1 models prefer low slip rates on the San Gorgonio Pass and Mojave segments of the SAF (< 10 mm/yr and 25-28 mm/yr); and high rates on the central section of the San Jacinto Fault, the Imperial Fault and the Coachella segment of the San Andreas fault (>13 mm/yr, 25-30 mm/yr and 35-40 mm/yr). Suite 2 models suggest low slip rates on the Coachella, central San Jacinto and Imperial faults (15-20 mm/yr, <10 mm/yr and 15-30 mm/yr). Figure 3 shows model sensitivity to slip rates on the S Mojave SAF and the Coachella SAF. Reducing locking depths on the Coachella, Imperial and central San Jacinto segments allows some overlap between admissible slip rate ranges for GPS- and strain energy-constrained models. However, further refinement of the model and efforts to reconcile these slip rates should take into account a possible active fault strand about 10 km west of the Imperial Fault (Lindsey and Fialko, 2016).

*Transverse Ranges.* All of the models strongly prefer a rate of convergence at the low end of the UCERF3 range for the Ventura-Oak Ridge fault system within the Transverse Ranges (i.e. 3 to 10 mm/yr; Figure 1). Slip rate ranges for the Ventura-Oak Ridge fault system estimated from the UCERF3 report are 1.5 to 15 mm/yr (summing rates for the Ventura/Pitas Point and Red Mountain faults) and 3.2 to 15 mm/yr (summing rates for the Oak Ridge and San Cayetano faults). My inferred slip rate (< 6 mm/yr) is consistent with the recent estimate from Hubbard et al. (2014) of 4.4 to 6.9 mm/yr.

*Effect of viscoelastic perturbation to the GPS velocity field.* Correcting the GPS velocity field for seismic cycle effects associated with the 1857 rupture segment of the SAF has a modest yet noticeable effect on slip rates inferred for the Mojave segment of the SAF (Figure 4). I corrected the CMM4 GPS velocity data using VISCO1D with earthquake parameters from Hearn et al. (2013). The SAF earthquake ruptures extended through a 25 km thick elastic upper plate and below this an effective viscosity of  $5 \times 10^{19}$  Pa s was assumed down to a depth of 270 km, where it was increased by a factor of ten. The perturbation relative to the interseismic average was added to the GPS field and used to constrain a slip rate inversion assuming locked faults (Suite 1a models). A higher slip rate (by about 4 mm/yr) is preferred for the Mojave segment of the SAF. For other fault segments the effect of the correction is more subtle.

*Off-fault deformation.* Contributions to present-day surface deformation arise from (1) interseismic, elastic locking of modeled faults, (2) “off-fault” deformation, and (3) viscoelastic earthquake-cycle and human-induced effects. As noted above, I have computed (3) using a viscoelas-

tic seismic cycle model and used this to adjust the SCEC CMM4 velocity field. One suite of locked models (Suite 1a) is calibrated to this field. An unlocked model suite set to minimize strain energy (Suite 2) should provide an estimate of off-fault deformation, and the best models in Suites 1a and 2 should have identical slip rates. A comparison of strain energy values in the upper crust for these two models provides the best self-consistent estimate of the proportion of strain energy that is not associated with locking of known, major faults. If seismic cycle effects are negligible, then a comparison of the best Suite 1 and Suite 2 models (presumably, with identical slip rates) should provide an accurate estimate of the off-fault strain energy budget in the upper crust.

I selected slip rate ranges for major faults in Suite 2 that were within the UCERF3 ranges, and for which at least one model had a minimum strain energy of less than  $6.6 \times 10^{18}$  J/y (counting model elements in southern California and adjoining areas). I refined the admissible slip rate ranges by finding Suite 1 models with slip rates in these ranges and a minimum normalized WRSS of less than 1.2. Strain energies from Suite 1 and Suite 2 models incorporating slip rates within the admissible ranges for both suites were compared. Using 11, MCMC-accepted Suite 1 models and 19 accepted Suite 2 models, I estimated mean strain energies (and standard deviations) of  $3.70 (\pm 0.30) \times 10^{19}$  N m/y and  $8.67 (\pm 1.20) \times 10^{18}$  N m/y respectively, and a ratio of  $0.23 (\pm 0.04)$ , meaning that about a quarter of the apparently accumulating strain energy is off-fault deformation. Doing the same exercise but with Suite 1a models, I obtain  $0.24 (\pm 0.04)$ . If I simply compare the best Suite 1 model (with WRSS = 1.0 and strain energy =  $2.0 \times 10^{19}$  N m/y) with the best Suite 2 model (with strain energy =  $6.0 \times 10^{18}$  N m/y and WRSS = 2.7), without requiring that they have consistent slip rates, I estimate that 32% of the strain energy is from off-fault deformation. Both estimates are consistent with other recent studies (e.g. Zeng and Shen, 2016).

### **Dynamic modeling**

My proposed dynamic model with deformation driven by side boundaries and solely the San Andreas Fault Zone switched on (and represented as a viscous shear zone) was run early in 2015, but it did not converge. This is because the “split node” (Melosh and Raefsky, 1981) method I use to model stress-driven fault creep, which works well for earthquake-cycle models and for fairly straight faults that completely cut the mesh, does not always converge for model faults with sharp kinks or discontinuities. Spurious local stresses (and slip rates) build up over time. To solve this problem, I revised the “slippery” fault node technique (Melosh and Williams, 1989) to enforce a specified, non-zero shear stress along the fault. I also decided that plasticity of the upper crust must be implemented before I attempt to model long-term deformation of southern California.

### **Plasticity**

I implemented plasticity using the predictor-corrector method, which is suitable for static long-term deformation problems. A Drucker-Prager rheology is assumed, though by eliminating dependence of the rheology on volumetric strain, I can model Von Mises plasticity as well. Plasticity parameters from Li et al. (2009) are adopted ( $\mu = 0.4$  and cohesion = 50 MPa, so plasticity pa-

parameters  $\alpha$  and  $k$  are 0.17 and 61 MPa, respectively). Simple tests with uniform strain throughout the modeled domain reproduce analytical stress solutions, but models in which a restraining bend is present give stresses that increase steadily with time. This is because increasingly compressive mean normal stresses prevent the plasticity yield condition from being met. I solve this problem using a “cap” function (e.g., Sandler and Rubin, 1979), in which an elliptical function closes the yield envelope at mean normal stresses exceeding 100 MPa, allowing plastic strain to occur in elements undergoing compression. The choice of cap function and its implementation details will require more justification and refinement because in regions undergoing compression (e.g. the Big Bend) they may exert a strong influence on modeled stresses. (Li et al. [2009] use a cap function in their California deformation models, but details are not provided.)

### Modified Slippery Nodes

I also modified the “slippery node” technique to allow (specified) non-zero shear tractions along an otherwise freely slipping fault. This is analogous to modeling stress-driven creep, though with a spatially varying viscous or plastic rheology enforcing a specified, constant shear stress along the fault. Such models produce more “well-behaved” slip distributions, and the computations are very rapid (for elastic Earth models, no time stepping is needed).

### SHmax

To aid in calibration of dynamic models, I have implemented comparison of maximum principal stress axis orientations (SHmax) with values from the SCEC CSM (from Yang and Hauksson [2013], called YH2013 from here on). Figure 5 summarizes how this was done. Since the YH2013 stress data are reported at regular, close-spaced intervals prescribed for the CSM, average values had to be computed at element centers for comparison with my FEM results. To do this I took the average of SHmax azimuths from all CSM points within each FE model element. The YH2013 azimuths vary in a patchy sense (Figure 5b) and values vary significantly within my FE model elements. For the example shown in Figure 5, the reported errors in SHmax orientation are less than 0.5 degree, but the standard deviation in within-element values is about 10 degrees. This method will be improved in 2016 by comparing the CSM SHmax values with within-element FEM values computed at Gauss points.

SHmax axes for a test model with an elastic lithosphere and zero-traction SAF are shown on Figures 5c and 5d. Significant misfits between this model and YH2013 arise in the western Mojave, in the Transverse Ranges and around bends in the SAF (the Big Bend and the Salton Sea region). A model with Drucker-Prager plasticity enabled (not shown on Figure 5) gives a superior fit to YH2013 in the Big Bend region and a poorer fit in the vicinity of the Landers and Hector Mine earthquakes. A model with shear resistance along the SAF does not significantly influence the SHmax orientations, but the resolved shear tractions in this model are low (about 5 MPa). Because these preliminary models incorporate solely the SAF, they are not expected to fit the SHmax orientations in detail.

For my funded 2016 NEHRP project, which is essentially a continuation of this one, I will use the SHmax misfit as a model calibration constraint, and will develop dynamic models of south-

ern California deformation making use of newly-implemented plasticity and modified slippery nodes.

## References

- Field, E. H. et al. (2013), Uniform California earthquake rupture forecast, version 3 (UCERF3) —The time-independent model, USGS Open-File Report 2013–1165, 97 pp., California Geological Survey Special Report 228, <http://pubs.usgs.gov/of/2013/1165/>.
- Hearn, E. H. et al. (2013), How do “ghost transients” from past earthquakes affect GPS slip rate estimates on southern California faults?. *Geochemistry, Geophysics, Geosystems*, 14(4), 828-838.
- Hubbard, J., J. H. Shaw, J. Dolan, T. L. Pratt, L. McAuliffe, and T. K. Rockwell (2014), Structure and seismic hazard of the Ventura Avenue anticline and Ventura fault, California: Prospect for large, multisegment ruptures in the Western Transverse Ranges, *Bull. Seis. Soc. Am.*, 104, 1070-1087.
- Johnson, K. (2013), Slip rates and off-fault deformation in Southern California inferred from GPS data and models, *J. Geophys. Res.*, 118, doi:10.1002/jgrb.50365.
- Li, Q., Liu, M., and Zhang, H. (2009), A 3-D viscoelastoplastic model for simulating long-term slip on non-planar faults, *Geophys. J. Int.*, 176(1), 293-306.
- Lindsey, E. O. and Y. Fialko (2016), Geodetic constraints on frictional properties and earthquake hazard in the Imperial Valley, Southern California, *J. Geophys. Res.* (online pre-pub Mar 2016).
- Melosh, H. J. and A. Raefsky (1981), A simple and efficient method for introducing faults into finite element computations. *Bull. Seis. Soc. Am.*, 71(5), 1391-1400.
- Melosh, H. J. and C. A. Williams (1989), Mechanics of graben formation in crustal rocks: A finite element analysis, *J. Geophys. Res.*, 94(B10), 13961-13973.
- Sandler, I. S. and D. Rubin (1979), An algorithm and a modular subroutine for the cap model, *Int. J. Num. and Analyt. Meth. Geomech.*, 3(2), 173-186.
- Saucier, F., and E. D. Humphreys (1993), Horizontal crustal deformation in Southern California from joint models of geologic and very long baseline interferometry measurements, in *Contrib. Space Geod. to Geodyn.*, vol. 3, D. E. Smith and D.L. Turcotte, eds., pp. 139–176, AGU Geodyn. Ser., Washington D. C.
- Yang, W. and E. Hauksson (2013), The tectonic crustal stress field and style of faulting along the Pacific North America Plate boundary in Southern California, *Geophys. J. Int.*, 194(1), 100-117.
- Zeng, Y. and Z. K. Shen (2016), A Fault-Based Model for Crustal Deformation, Fault Slip Rates, and Off-Fault Strain Rate in California, *Bull. Seis. Soc. Am.*, online pre-pub Mar 2016.

## Bibliography

- Hearn, E. H., Kinematic Models of Southern California Deformation calibrated to GPS Velocities and a Strain Energy Minimization Criterion: How do they Differ?, American Geophysical Union 2015 Fall Meeting Abstract T41A-2865, Dec 17, 2015.
- A manuscript describing the kinematic modeling is in preparation.

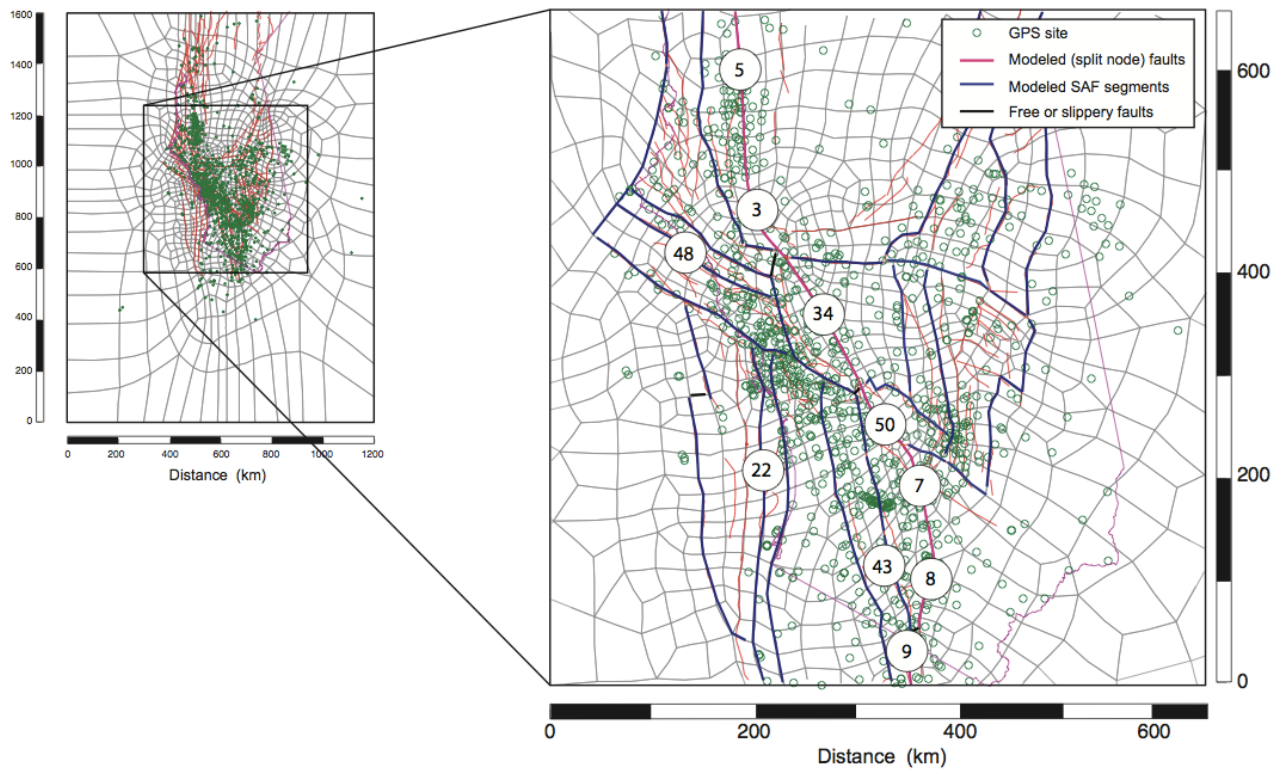


**Figure 1.** Finite element model mesh with inset detail. Block bounding faults are blue lines (red for the SAF system). Green circles denote SCEC CMM4 stations. Numbers denote some of the modeled fault segments. 3 and 34: N and S Mojave SAF, 8: Coachella SAF, 9: Imperial Fault, 48: Ventura Oak-Ridge Fault, 50: San Gorgonio SAF.

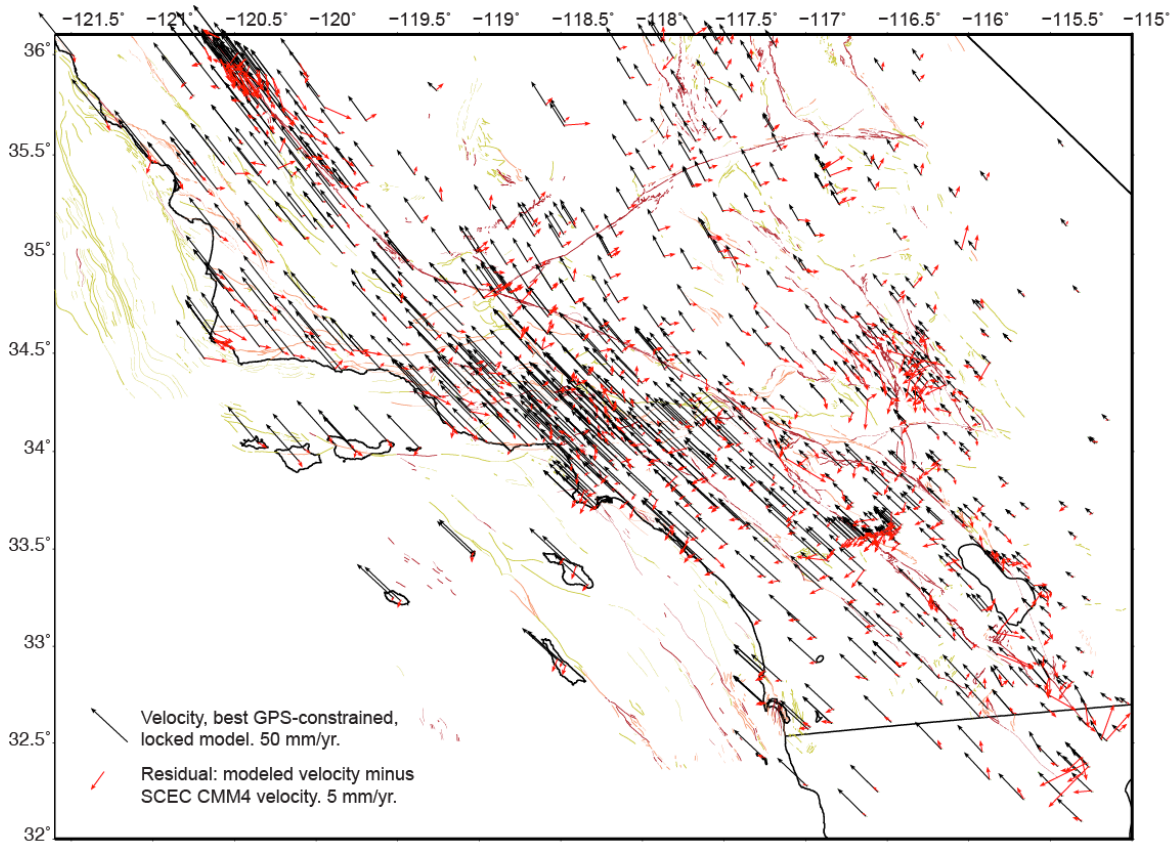
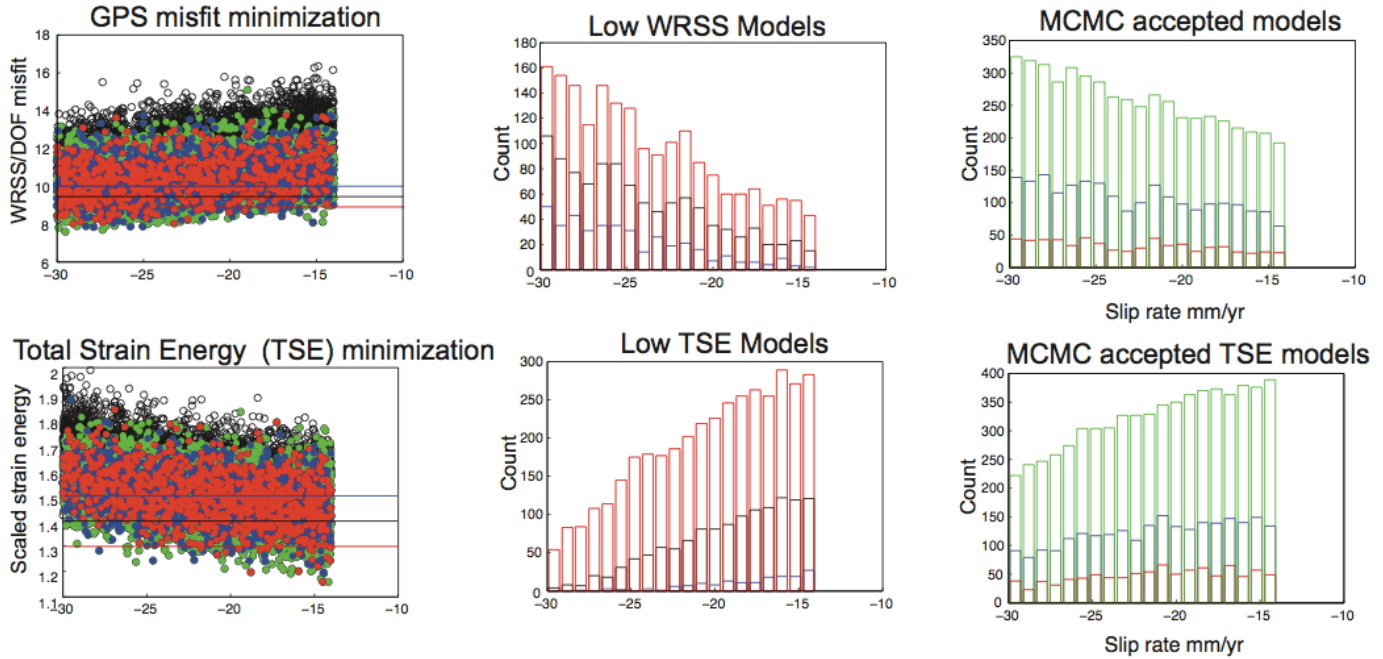
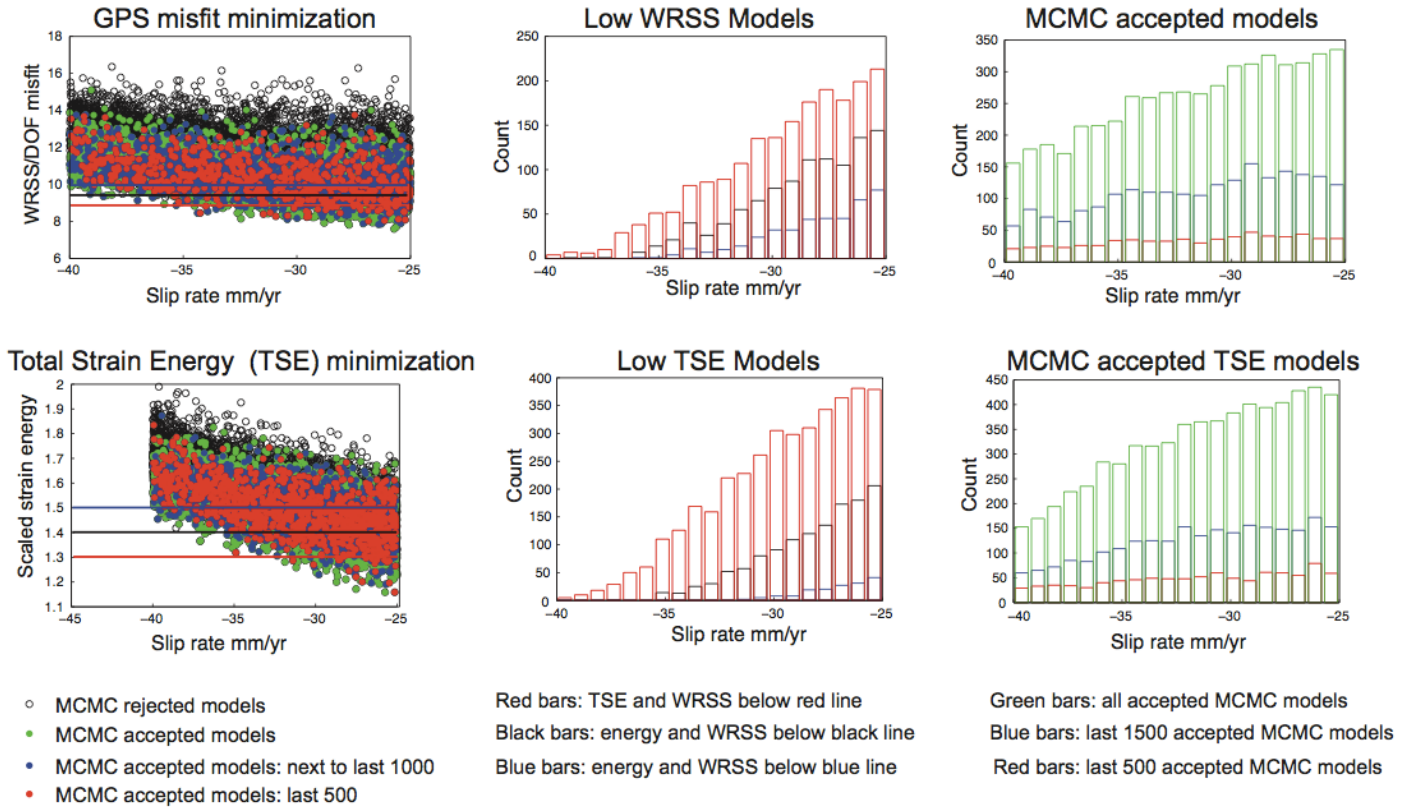


**Figure 2.** Modeled velocities (black) and residuals (red) for best-fitting locked (Suite 1) models.

### Coachella Fault (model segment 8)



### South Mojave SAF (model segment 34)



- MCMC rejected models
- MCMC accepted models
- MCMC accepted models: next to last 1000
- MCMC accepted models: last 500

- Red bars: TSE and WRSS below red line
- Black bars: energy and WRSS below black line
- Blue bars: energy and WRSS below blue line

- Green bars: all accepted MCMC models
- Blue bars: last 1500 accepted MCMC models
- Red bars: last 500 accepted MCMC models

**Figure 3.** Sensitivity of WRSS misfit to GPS velocity data, and total strain energy (TSE), to slip rates on individual fault segments. For the Coachella fault (top), these measures point to different slip rates while for the southern Mojave segment, both suggest a low slip rate. Bar charts show hit counts of models with misfit below the indicated thresholds (center) and accepted models (right), as a function of slip rate.

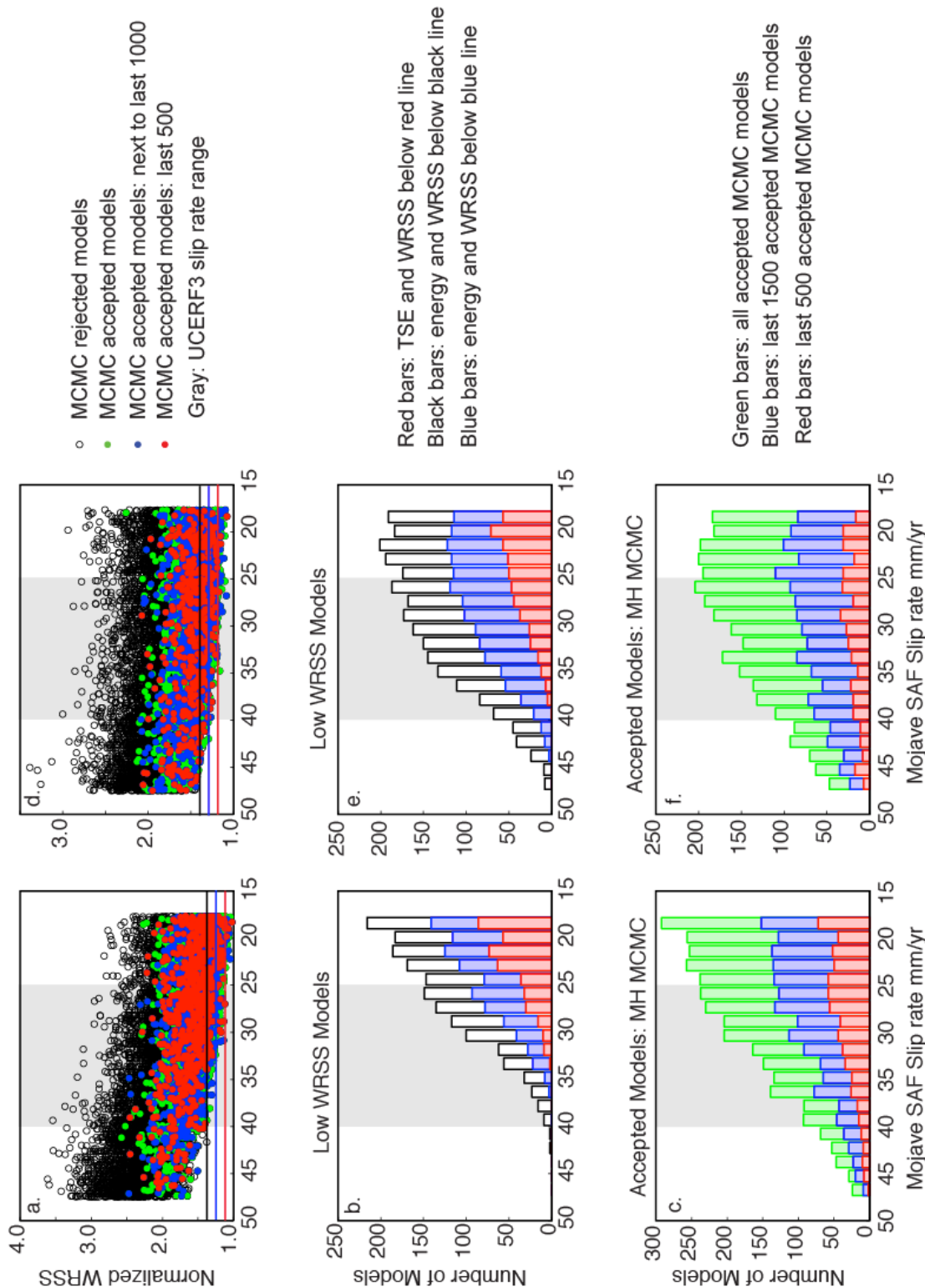


**Figure 4.** Results from two kinematic model suites, showing the how seismic cycle effects may influence inferred slip rates along the Mojave SAF (segment 34). Panels a and d show the fit to GPS velocities as a function of slip rate on this fault segment, for locked models calibrated to the SCEC CMM4 GPS velocity field without (a) and with (c) a correction for viscoelastic seismic cycle effects (see text). The fit is represented as the weighted residual sum of squares (WRSS) normalized to the lowest WRSS on panel a. Panels c and f show slip rate distributions for models with WRSS and strain energy rate below thresholds indicated with the colored lines on panels a and b. Panels e and f show distributions of slip rates for accepted models, for the Metropolis-Hastings MCMC method. 10,000 models were run in each case and the acceptance rate was about 35%. Gray shading shows the UCERF3 slip rate range.

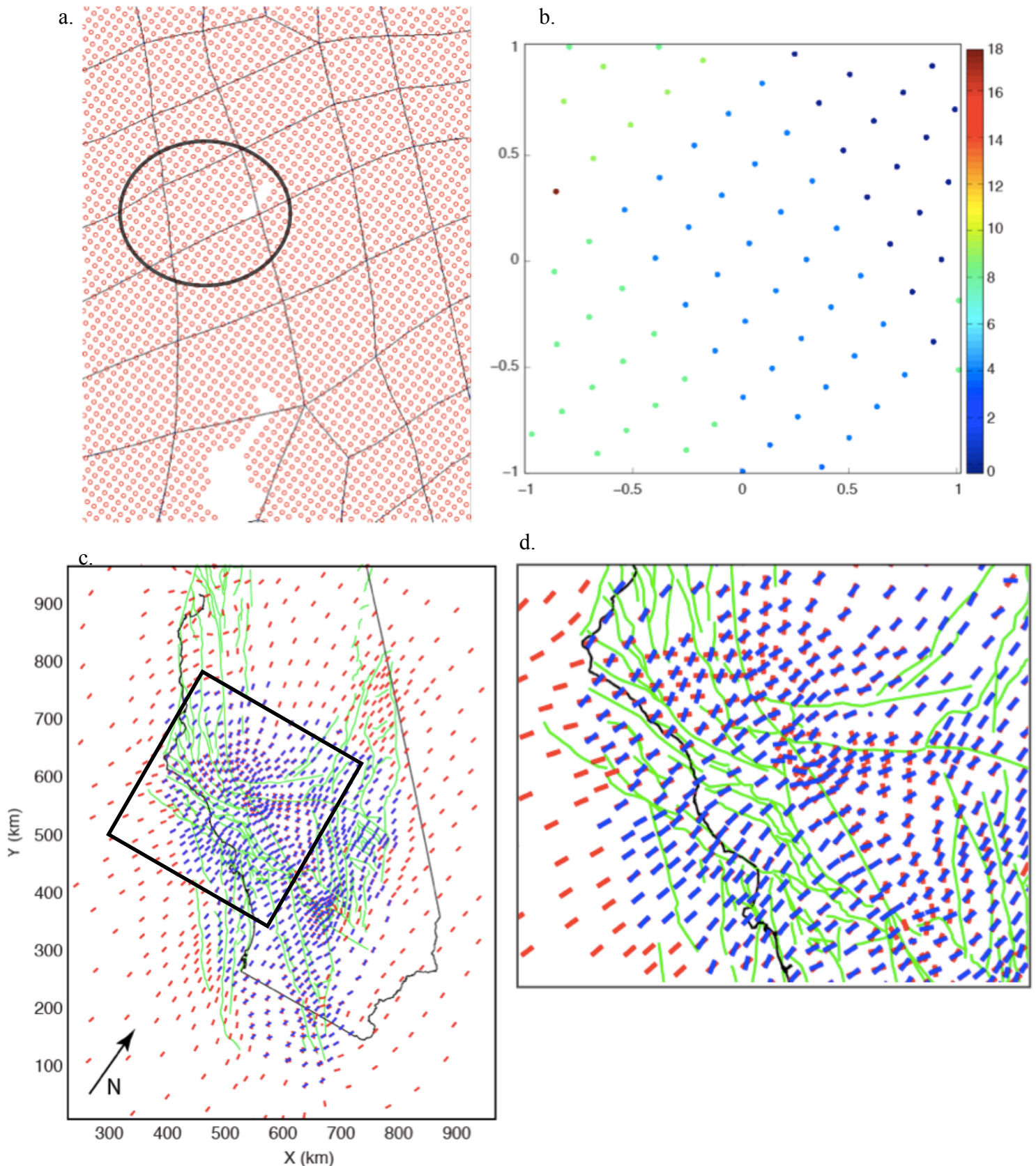


**Figure 5.** a. SCEC Community Stress Model (CSM) grid points superimposed on part of the finite element model mesh. b. Values of SHmax azimuths (Yang and Hauksson, 2013 [YH2013]) at grid points in one model element (circled on a), in local coordinates. Note variation and patchiness. c. Model SHmax orientations at element centers (red) and YH2013 SHmax orientations averaged over element volumes. All are scaled to the same length (some are not horizontal). Element centers are at  $z = 5$  km. d. Zoomed in view of c. Note poor fit at SAF Big Bend and in the western Mojave. See text for model details.